

This work was written as part of one of the author's official duties as an Employee of the United States Government and is therefore a work of the United States Government. In accordance with 17 U.S.C. 105, no copyright protection is available for such works under U.S. Law.

Public Domain Mark 1.0

<https://creativecommons.org/publicdomain/mark/1.0/>

Access to this work was provided by the University of Maryland, Baltimore County (UMBC) ScholarWorks@UMBC digital repository on the Maryland Shared Open Access (MD-SOAR) platform.

Please provide feedback

Please support the ScholarWorks@UMBC repository by emailing scholarworks-group@umbc.edu and telling us what having access to this work means to you and why it's important to you. Thank you.

Excitation of Dark Plasmons in Metal Nanoparticles by a Localized Emitter

Mingzhao Liu (刘铭钊),^{1,2,*} Tae-Woo Lee,^{3,†} Stephen K. Gray,³ Philippe Guyot-Sionnest,¹ and Matthew Pelton^{2,‡}

¹*James Franck Institute, The University of Chicago, Chicago, Illinois 60637, USA*

²*Center for Nanoscale Materials, Argonne National Laboratory, Argonne, Illinois 60439, USA*

³*Chemical Sciences and Engineering Division, Argonne National Laboratory, Argonne, Illinois 60439, USA*

(Received 20 June 2008; published 9 March 2009)

We study theoretically a dipole emitter placed near a metal nanoparticle and near small chains of two and three nanoparticles. The emitter can efficiently excite dark, or nonradiative, surface-plasmon modes in the nanostructures, in addition to the well-known bright modes. In the case of coupled nanoparticles, the origins of the bright and dark modes can be understood in the context of plasmon hybridization. Excitation of dark modes in nanoparticle chains allows for subwavelength guiding of optical energy with no radiative losses and thus with improved propagation lengths.

DOI: 10.1103/PhysRevLett.102.107401

PACS numbers: 78.67.Bf, 78.45.+h, 78.68.+m

Metal nanoparticles have the ability to strongly modify optical emission from localized emitters. They act as the optical analogue of resonant radio or microwave antennas, enhancing and broadcasting radiation through the excitation of localized surface plasmons. This effect has long been considered as an explanation for enhancement of Raman scattering by metal nanostructures [1] and has also been demonstrated to modify the fluorescence from isolated molecules [2,3]. Enhanced emission can be considered the complement of enhanced absorption, where excitation of a plasmon resonance is used to localize incident radiation to length scales well below the diffraction limit, leading to efficient excitation of a nearby dipole. In this case, provided the dimensions of the nanoparticle are much smaller than the radiation of the incident radiation (that is, less than about 100 nm), only dipolar plasmon resonances can be excited. It is often assumed that this same limit, known as the quasistatic approximation, can be used to understand enhanced emission [4–6]. More detailed calculations have shown that localized dipoles can excite higher-order, multipolar plasmon modes in nanoparticles, leading to quantitative changes in emission rates [7,8]. For the spherical particles considered, though, the higher-order modes are strongly damped and overlap with the lowest-order dipolar mode, so that their influence on emission is relatively minor.

In this Letter, we use rigorous electrodynamic modeling to show that the coupling of a localized dipole to certain metal nanostructures is qualitatively different from the coupling of far-field radiation. In particular, the dipole can excite dark-plasmon modes that do not radiate and do not couple to incident plane waves. These dark modes include quadrupolar modes in single nanoparticles, coupled modes in nanoparticle pairs, and propagating modes in nanoparticle chains. The dark propagating modes allow for waveguiding on length scales much smaller than the diffraction limit [9,10], with no radiative losses.

The first case we consider is a dipole emitter interacting with a bipyramidal gold nanoparticle. Such particles can be

experimentally synthesized as colloids with high monodispersity [11], and their pointed shapes lead to significant localization of incident fields [12]. In addition, their shape can be controlled such that the plasmon resonances lie far from interband transition energies, reducing their damping. A real nanoparticle is accurately modeled as a pentagonal bipyramid whose length is 83.4 nm, whose equatorial radius is 15 nm, and whose tips are truncated by hemispheres with a curvature of 3 nm [12]. The gold bipyramid is assumed to be immersed in water (dielectric constant = 1.77). The dipole source is placed along the major axis of the bipyramid (designated as the z axis), 13 nm from the nanoparticle tip, and is polarized in the z direction.

We model the system using three-dimensional finite-difference time-domain (FDTD) calculations [13,14]. The optical constants of the metals are approximated by a Lorentz-Drude model, as described in Ref. [12], with parameters adjusted to fit the experimental values measured by Johnson and Christy [15]. The radiative source is treated as an oscillating classical point dipole, $\mathbf{p}(t)$, generated by introducing a current density $\mathbf{j}(t) \propto d\mathbf{p}(t)/dt$ at the desired spatial grid point. We take $\mathbf{p}(t)$ to be a sinusoidal pulse with energy content in the 1–4 eV range. Fourier transforms of the time-dependent electromagnetic fields allow construction of the frequency-dependent Poynting vector, $\mathbf{S}(\omega)$, on various surfaces. Letting $\Gamma_0(\omega)$, $\Gamma_r(\omega)$, and $\Gamma_{nr}(\omega)$ be the isolated dipole radiative rate and the radiative and nonradiative decay rates for the full system, respectively, the relative decay rates Γ_r/Γ_0 and Γ_{nr}/Γ_0 are then given by ratios of powers inferred from surface integrals over \mathbf{S} : $\Gamma_r/\Gamma_0 = W_r/W_0$ and $\Gamma_{nr}/\Gamma_0 = -W_{nr}/W_0$ [16,17]. The radiated power of the isolated dipole system is $W_0(\omega) = \iint_{\Sigma_0} \mathbf{S}_0(\omega) \cdot d\mathbf{\Sigma}$, where Σ_0 is a surface enclosing the dipole and \mathbf{S}_0 is the Poynting vector in the absence of the metal nanoparticle(s). The radiative and nonradiative powers in the presence of the nanoparticle(s) are $W_r(\omega) = \iint_{\Sigma_1} \mathbf{S}(\omega) \cdot d\mathbf{\Sigma}$, where Σ_1 encloses the dipole and nanoparticle(s), and $W_{nr}(\omega) = \iint_{\Sigma_2} \mathbf{S}(\omega) \cdot d\mathbf{\Sigma}$, where Σ_2 encloses only the nanoparticle(s).

The simulation results are shown in Fig. 1(a). Also shown, for comparison, is the calculated cross section for absorption by the metal nanoparticle of incident plane-wave radiation. The radiative rate is enhanced by more than 70 times at the longitudinal dipolar plasmon resonance energy of 1.5 eV, and a nonradiative decay rate maximum is also observed at this energy. A second peak is observed at 1.75 eV in the nonradiative decay rate but is absent in the radiative decay and in the far-field absorption [18]. If the dipole is moved closer to the bipyramid, this peak becomes larger, but its energy and width are unchanged. We note that there is also a weak absorption feature at approximately 2.0 eV, corresponding to a higher-order mode in which the fields are primarily localized at the tips of the particles. In the following, only the two lower-energy modes are considered.

The nature of these modes is identified by examining the distribution of the electric field at the peak energies, as shown in Figs. 1(b) and 1(c). For the lower-energy mode, the polarization is along the same direction throughout the bipyramid, indicating that this is a dipolar mode. For the higher-energy mode, on the other hand, the polarization

changes direction from one side of the particle to the other, and polarization charges with the same sign appear on both tips at the same time, indicating that this is a quadrupolar mode. Because of the small size of the bipyramid compared to the optical wavelength, phase retardation is minimal, and the net dipole moment is nearly zero. The quadrupolar mode is thus dark: it does not couple to far-field radiation. For this reason, even though the field enhancement near the tips is nearly as large as for the dipolar mode, radiative enhancement is absent.

Dark plasmons can also arise as a result of the coupling between multiple metal nanoparticles. For example, when two nanoparticles are brought together, their individual plasmon resonances interact through electrostatic forces, forming new, collective resonances. An intuitive picture of this interaction is given by the plasmon-hybridization model, which provides a formal analogy to chemical bonding: individual, atomic-orbital-like plasmon modes combine to form coupled, molecular-orbital-like modes [19]. The hybrid modes correspond to symmetric (bonding) and antisymmetric (antibonding) combinations of the individual modes [20]. While the lower-energy, bonding mode interacts strongly with incident radiation, the higher-energy, antibonding mode has nearly zero net dipole moment, and is thus dark. Although the dark mode has therefore been safely neglected when considering coupling to incident far-field radiation, it must be included when considering emission modification, since it can couple to a localized dipole as strongly as the bright mode.

To demonstrate this, we consider a pair of prolate ellipsoidal silver nanoparticles, aligned along their major axes (the z axis). Although we calculated similar effects for a pair of gold bipyramids, the silver ellipsoids allow for explicit comparison to the hybridization model, because analytical solutions can be developed for the relevant charge densities, and because silver is a nearly ideal Drude metal at the plasmon resonance frequencies of interest. The ellipsoids considered have diameters of 10 nm and aspect ratios of 4.5 and are separated by a 5-nm gap. The dipole is placed on the z axis, 5 nm from one of the ellipsoids, and is z polarized. This placement of the dipole removes the inversion symmetry of the system, so that it is possible to excite both symmetric and antisymmetric hybridized modes of the nanoparticle pair. When illuminated by a plane wave, a single ellipsoid has a longitudinal (z -polarized) plasmon resonance at 2.08 eV, which is slightly lower than the 2.15 eV value expected from Gans' quasistatic theory [21]. The bright resonance shifts to 1.98 eV for the ellipsoid pair [Fig. 2(a)]. At this energy, the radiative rate of the dipole is enhanced by approximately 1000 times and there is also a significant nonradiative enhancement. Another nonradiative peak is present at 2.16 eV, with similar amplitude and line shape. As in the single-particle case, there is no radiative enhancement and no far-field absorption at the dark-plasmon energy. At yet higher energies, around 2.7 eV, there is a double peak in the nonradiative enhancement, corresponding to the symmet-

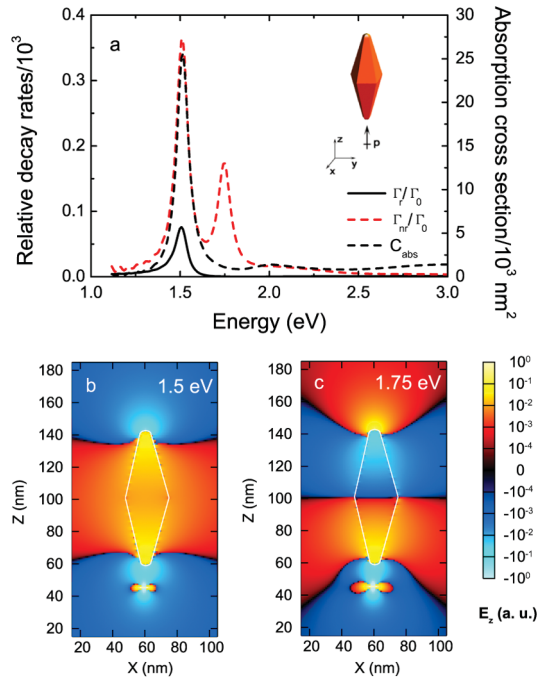


FIG. 1 (color). (a) Radiative enhancement Γ_r/Γ_0 (solid black line) and nonradiative enhancement Γ_{nr}/Γ_0 (dashed red line) of a point dipole by a gold bipyramid. The configuration of the system is shown in the inset. Also shown is the optical absorption cross section, C_{abs} , of the gold bipyramid (dashed black line). (b) The z component of the electric field on the x - z plane (through the center of the bipyramid) containing a dipole radiating at 1.5 eV, coupled to the dipolar mode of the nanoparticle. The emitting dipole is located at $x = 60$ nm, $z = 45$ nm. The solid white line indicates the boundary of the nanoparticle. (c) The same plot as (b), but for emission at 1.75 eV, coupled to the quadrupolar mode of the nanoparticle.

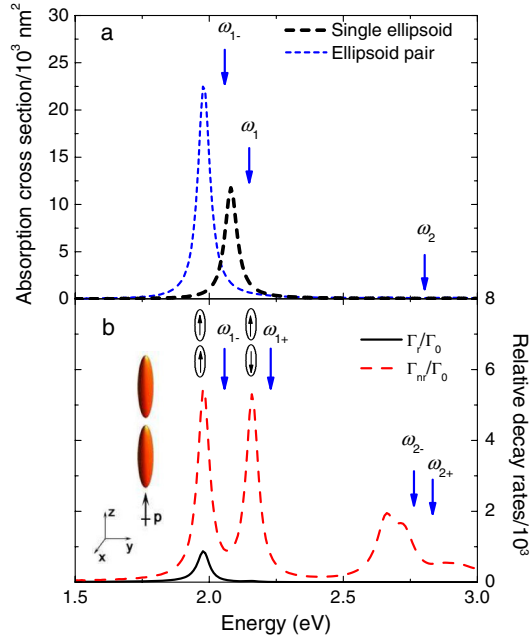


FIG. 2 (color online). (a) Optical absorption spectra of a single silver ellipsoid (thin dashed line) and a pair of ellipsoids (thick dashed line). The polarization of light is along the major axes of the ellipsoids. (b) Radiative enhancement Γ_r/Γ_0 (solid line) and nonradiative enhancement Γ_{nr}/Γ_0 (dashed line) of a point dipole by a pair of silver ellipsoids in its vicinity. The system configuration is shown in the inset. The arrows show the resonant energies from electrostatic models. ω_1 and ω_2 correspond to the dipolar and quadrupolar modes, respectively, and are obtained from the quasistatic approximation. $\omega_{1\pm}$ and $\omega_{2\pm}$ are the corresponding bonding and antibonding modes, and are obtained from the plasmon-hybridization model.

ric and antisymmetric combinations of the single-particle quadrupolar resonances.

Identification of the modes was verified by calculating the expected energies according to the plasmon-hybridization model, expanding the surface charge density on the nanoparticles in prolate ellipsoidal coordinates [22]. The predicted energies of the bonding and antibonding states are 2.06 and 2.23 eV, respectively. The peak splitting is in excellent agreement with the FDTD calculations, as shown in Fig. 2(b). Similarly good agreement is obtained for the combination of the quadrupolar modes.

When more than two metal nanoparticles are coupled together, the number of hybrid states increases, eventually merging into bands for long nanoparticle chains. A localized dipole at the end of the chain can couple to propagating states in these bands, leading to the transport of electromagnetic energy along a waveguide whose dimensions are small compared to the diffraction limit [23,24]. The bright plasmon modes will evolve into radiant modes, while the dark-plasmon modes will evolve into subradiant modes, for which radiative losses are eliminated. This, in turn, improves propagation lengths, potentially facilitating applications such as integration with other nanoscale elements and image transfer below the diffraction limit.

As an illustrative example, we consider a short chain of three coupled nanoparticles, returning to the consideration of gold bipyramids. The configuration, shown in Fig. 3(a), is similar to the single-bipyramid case, with two more nanoparticles placed on the opposite side from the point dipole, and with 10 nm tip-to-tip distance between each pair of bipyramids. Based on the plasmon-hybridization picture, the dipolar mode of an isolated particle is expected to be split into three modes for the three-particle chain; in analogy to molecular orbitals, these can be labeled as bonding, nonbonding, and antibonding. Only the bonding mode is expected to be bright, and, indeed, the calculations show that only the lowest-energy mode, at 1.41 eV, produces significant far-field absorption and radiative enhancement [see Fig. 3(a)]. The other two modes, located at 1.51 and 1.59 eV, are dominated by nonradiative dis-

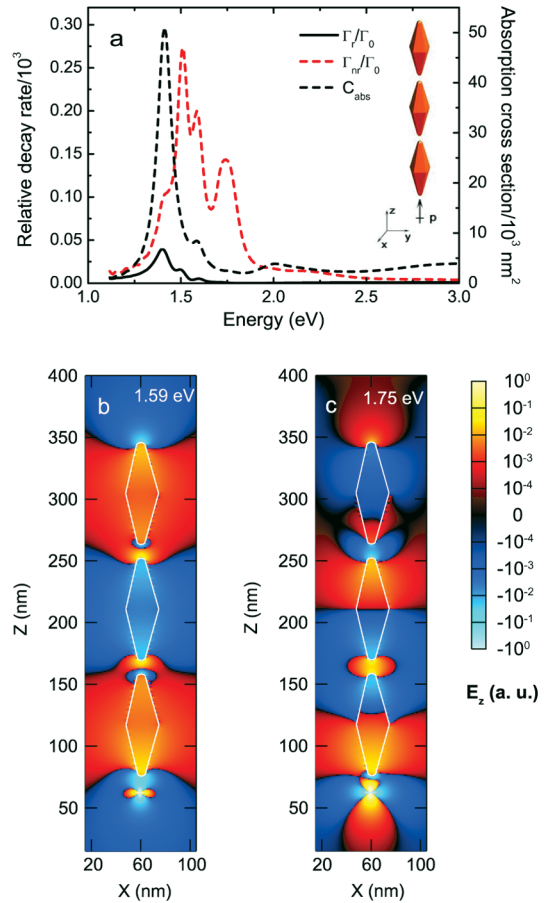


FIG. 3 (color). (a) Radiative enhancement Γ_r/Γ_0 (solid black line) and nonradiative enhancement Γ_{nr}/Γ_0 (dashed red line) of a point dipole by a chain of three gold bipyramids in its vicinity. Also shown is the optical absorption cross section, C_{abs} , of the gold bipyramid chain (dashed black line). (b) The z component of the electric field on the x - z plane containing the dipole radiating at 1.59 eV, coupled to the antibonding dipolar mode of the chain. The radiative dipole is located at $x = 60$ nm, $z = 62$ nm. The solid white lines indicate the boundaries of the nanoparticles. (c) The same plot as (b), but for radiation at 1.75 eV, coupled to the quadrupolar mode.

sipation. This is also true for the quadrupolar mode at 1.75 eV; for this mode, the splitting between the three hybrid states is smaller than the linewidth, and a broadened peak is seen instead of three separate peaks.

Propagation of the dark modes can be visualized by plotting the electric field. For the antibonding mode, shown in Fig. 3(b), the electric field is delocalized along the 300-nm chain. The phase of the field is homogeneous across each bipyramid but changes by about π from one nanoparticle to its neighbor, which greatly reduces the radiation to the far field. One can approximate the propagation length of the plasmon as $D = d_{13} / \ln(|\mathbf{E}_1|^2 / |\mathbf{E}_3|^2)$, where \mathbf{E}_1 and \mathbf{E}_3 are the electric field amplitudes at the centers of the first and third bipyramids, respectively, and d_{13} is the distance between their centers. The propagation length for the antibonding mode is found to be 188 nm. For the 1.41 eV bonding mode, the propagation length is reduced to 169 nm, reflecting the additional radiative loss. The longest propagation length, of 260 nm, is seen for the 1.51 eV nonbonding mode; compared with the bonding mode, elimination of radiative losses provides an increase of over 50% in the propagation distance. Optimization of the nanoparticle geometry, spacing, and material should make it possible to reduce nonradiative losses, as well, allowing for long-range energy transfer along nanoparticle chains.

A similar plot is shown in Fig. 3(c) for the quadrupolar mode at 1.75 eV. The propagation length for this mode of 58 nm is still significant, considering that the propagation is due to the quadrupole-quadrupole interaction, which is much weaker than the dipole-dipole interaction. Indeed, the propagation length is only approximately 40% less than that recently measured for coupled dipolar modes [10]. One would expect stronger coupling, and, thus, longer propagation lengths upon reduction of the gaps between the nanoparticles. On the other hand, reducing the gaps beyond a certain point will lead to mixing of the quadrupolar modes with the dipolar modes, potentially increasing radiative losses.

In summary, we studied theoretically a dipole emitter placed in the near field of a metal nanoparticle and nanoparticle chains. In addition to large radiative enhancements due to coupling to bright surface-plasmon resonances, we found strong coupling to dark-plasmon modes that cannot be excited with incident light and that do not radiate to the far field. Consideration of these dark modes will be essential in understanding the modification of emission from molecules and semiconductors as well as other radiative processes, such as Raman scattering. Furthermore, we demonstrated that coupling to dark-plasmon modes allows for propagation along sub-diffraction-limited nanoparticle chains without any radiative losses, which may play an important role in future integrated nanophotonic devices. The elimination of radiative losses could also be favorable for other plasmonic applications, such as the achievement of nanoscale plasmon “lasing” [25].

M.Z.L. was supported by the University of Chicago MRSEC NSF-DMR under Grant No. DMR-0213745.

Work at the Center for Nanoscale Materials was supported by the U. S. Department of Energy, Office of Science, Office of Basic Energy Sciences, under Contract No. DE-AC02-06CH11357.

*liu13@fas.harvard.edu; Present address: Department of Chemistry and Chemical Biology, Harvard University, Cambridge, MA 02138

[†]Present address: Center for Computation and Technology, Louisiana State University, Baton Rouge, LA 70803

[‡]pelton@anl.gov

- [1] M. Moskovits, *J. Raman Spectrosc.* **36**, 485 (2005).
- [2] P. Anger, P. Bharadwaj, and L. Novotny, *Phys. Rev. Lett.* **96**, 113002 (2006).
- [3] S. Kühn, U. Håkanson, L. Rogobete, and V. Sandoghdar, *Phys. Rev. Lett.* **97**, 017402 (2006).
- [4] J. Gersten and A. Nitzan, *J. Chem. Phys.* **75**, 1139 (1981).
- [5] H. Mertens, A. F. Koenderink, and A. Polman, *Phys. Rev. B* **76**, 115123 (2007).
- [6] P. Bharadwaj and L. Novotny, *Opt. Express* **15**, 14266 (2007).
- [7] R. Rupp, *J. Chem. Phys.* **76**, 1681 (1982).
- [8] J.-Y. Yan, W. Zhang, S. Duan, X.-G. Zhao, and A. O. Govorov, *Phys. Rev. B* **77**, 165301 (2008).
- [9] M. L. Brongersma, J. W. Hartman, and H. A. Atwater, *Phys. Rev. B* **62**, R16356 (2000).
- [10] S. Maier, P. G. Kik, H. A. Atwater, S. Meltzer, E. Harel, B. E. Koel, and A. A. G. Requicha, *Nature Mater.* **2**, 229 (2003).
- [11] M. Z. Liu and P. Guyot-Sionnest, *J. Phys. Chem. B* **109**, 22192 (2005).
- [12] M. Z. Liu, P. Guyot-Sionnest, T.-W. Lee, and S. K. Gray, *Phys. Rev. B* **76**, 235428 (2007).
- [13] K. S. Yee, *IEEE Trans. Antennas Propag.* **14**, 302 (1966).
- [14] A. Taflov and S. C. Hagness, *Computational Electrodynamics: The Finite-Difference Time-Domain Method* (Artech House, Boston, 2000), 2nd. ed.
- [15] P. B. Johnson and R. W. Christy, *Phys. Rev. B* **6**, 4370 (1972).
- [16] Y. Xu, R. K. Lee, and A. Yariv, *Phys. Rev. A* **61**, 033807 (2000).
- [17] F. Kaminski, V. Sandoghdar, and M. Agio, *J. Comp. Theor. Nanosci.* **4**, 635 (2007).
- [18] L. Rogobete, F. Kaminski, M. Agio, and V. Sandoghdar, *Opt. Lett.* **32**, 1623 (2007).
- [19] E. Prodan and P. Nordlander, *J. Chem. Phys.* **120**, 5444 (2004).
- [20] P. Nordlander, C. Oubre, E. Prodan, K. Li, and M. Stockman, *Nano Lett.* **4**, 899 (2004).
- [21] R. Gans, *Ann. Phys. (Leipzig)* **352**, 270 (1915).
- [22] D. W. Brandl and P. Nordlander, *J. Chem. Phys.* **126**, 144708 (2007).
- [23] A. F. Koenderink and A. Polman, *Phys. Rev. B* **74**, 033402 (2006).
- [24] A. F. Koenderink, R. de Waele, J. C. Prangsma, and A. Polman, *Phys. Rev. B* **76**, 201403 (2007).
- [25] D. J. Bergman and M. I. Stockman, *Phys. Rev. Lett.* **90**, 027402 (2003).